Title

Visualizing mechanical modulation of nanoscale organization of cell-matrix adhesions

Permalink

Journal

ISSN

Authors

Ou, Guanqing
Thakar, Dhruv
Tung, Jason C
et al.

Publication Date

DOI

Visualizing mechanical modulation of nanoscale organization of cell-matrix adhesions

Guanqing Ou[a,b], **Dhruv Thakar**[b], **Jason C. Tung**[b], **Yekaterina A. Miroshnikova**[a,b], **Christopher C. Dufort**[b], **Edgar Gutierrez**[c], **Alex Groisman**[c], and **Valerie M. Weaver**[b,d,e,f]

[a]University of California, Berkeley and University of California, San Francisco Joint Graduate Group in Bioengineering, San Francisco, CA, USA

[b]Center for Bioengineering and Tissue Regeneration, Department of Surgery, UCSF, San Francisco, CA, USA

[c]Department of Physics, UC San Diego, San Diego, CA, USA

[d]Department of Anatomy, and Department of Bioengineering and Therapeutic Sciences, UCSF, San Francisco, CA, USA

[e]Eli and Edythe Broad Center of Regeneration Medicine and Stem Cell Research, UCSF, San Francisco, CA, USA

[f]UCSF Helen Diller Comprehensive Cancer Center, UCSF, San Francisco, CA, USA

Abstract

The mechanical properties of the extracellular matrix influence cell signaling to regulate key cellular processes, including differentiation, apoptosis, and transformation. Understanding the molecular mechanisms underlying mechanotransduction is contingent upon our ability to visualize the effect of altered matrix properties on the nanoscale organization of proteins involved in this signaling. The development of super-resolution imaging techniques has afforded researchers unprecedented ability to probe the organization and localization of proteins within the cell. However, most of these methods require use of substrates like glass or silicon wafers, which are artificially rigid. In light of a growing body of literature demonstrating the importance of mechanical properties of the extracellular matrix in regulating many aspects of cellular behavior and signaling, we have developed a system that allows scanning angle interference microscopy on a mechanically tunable substrate. We describe its implementation in detail and provide examples of how it may used to aide investigations into the effect of substrate rigidity on intracellular signaling.

Graphical Abstract
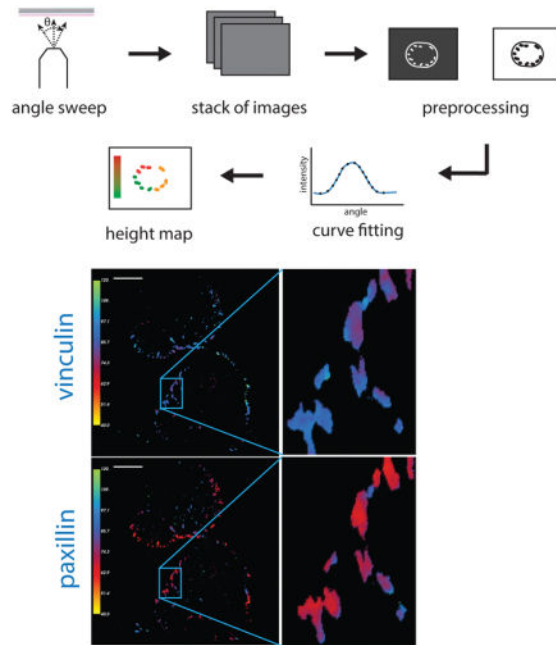
We present a novel platform for superresolution imaging of adhesion proteins on physiologically relevant substrates.

Introduction

Mechanical cues influence cell and tissue phenotype through a process termed mechanotransduction, in which receptors that bind extracellular matrix (ECM) molecules connect the cytoskeleton to the ECM and transduce information about the properties of the ECM via downstream signalling. This signalling can then induce changes in cell behaviour and fate. Engler *et al.* and Paszek *et al.* separately demonstrated the key role played by mechanical properties of the ECM in directing stem cell differentiation and malignant transformation, respectively.[1,2] Altering ECM stiffness can change cell proliferation, apoptosis, protein biogenesis, transcription, and more.[3–5] Researchers have made great strides in mechanistic understanding of this process with conventional cell and molecular biology approaches, which depend upon genetic mutants to elucidate the role played by various proteins in mechanotransduction[6,7]. Similarly, the employment of hydrogels and light microscopy has provided insight into how changing ECM properties influences subcellular organization of proteins.[8,9] More detailed mechanistic revelations, however, are contingent on our ability to visualize protein localization and interactions at a nanoscale level.

Super-resolution imaging has filled this need and permitted researchers to pinpoint the location of a labelled protein within the cell with nanometer precision. These methods have yielded studies that lend otherwise unattainable insight into the behaviour and organization of proteins within the cell. For example, Shroff *et al.* used photo-activated localization microscopy (PALM) to illustrate how paxillin is recruited to and disassociates from focal

adhesion complexes.[10] Scanning angle interference microscopy (SAIM) led to characterization of how a bulky glycocalyx drives integrin clustering independent of actomyosin contractility.[11,12] As interest in employing these methods to answer various biological questions grows, however, the need to adapt these techniques for biologically relevant experimental conditions arises. Cell and tissue elastic modulus can vary across multiple orders of magnitude, depending on type and location within the body.[1] The ability to mechanically tune the cell substrate *in vitro* can thus significantly enhance the physiological relevance of a study in question. As such, the ability to perform super-resolution imaging on mechanically tunable substrates would open up a new avenue of investigation and facilitate greater understanding of the molecular mechanisms underlying mechanical regulation of cell signalling and behaviour.

Here, we report a novel approach to perform scanning angle interference microscopy (SAIM) for nanoscale imaging of subcellular components on mechanically tunable substrates. This system offers nanoscale precision in pinpointing fluorophore localization while affording control over the mechanical properties of the cell substrate. We provide detailed description of this novel imaging approach, key changes to optical theory and associated image analysis software, validation of the gel properties and cellular responses, and example applications for the platform in imaging cell-matrix adhesions. This method has great potential for adaptation in any study where ECM rigidity may play a role and allows researchers to benefit from advances in technology without sacrificing physiological relevance.

Experimental Setup

In this section, we describe the experimental setup involved in utilizing this imaging platform, from silicone gel coating onto the imaging surface to image acquisition and analysis.

SAIM Background

Scanning angle interference microscopy is described in detail by Paszek *et al.*[13] To provide context for the steps detailed below, we briefly describe its origins and underlying theory here.

SAIM is an improvement of fluorescence interference contrast microscopy (FLIC), which uses surface-generated structured illumination to achieve z-super resolution.[14] In traditional FLIC, silicon wafers with different thickness silicon oxide layers are used. The interference pattern generated when light is reflected from these surfaces interacts with fluorophores situated on oxide layers of different thicknesses in predictable patterns.[14] For example, a fluorophore at a height corresponding with constructive interference will register higher fluorescence intensity than a fluorophore at a height corresponding with destructive interference. By assembling data about these fluorophores' relative positioning to the interference pattern, it is possible to calculate their absolute height above an imaging surface.[15] In SAIM, on the other hand, vertically varied patterns of illumination are generated by changing the incidence angle of excitation (Figure 1c).[13] As with FLIC, a

silicon wafer with a defined thickness of silicon oxide is used. However, in SAIM, only one thickness is needed, thereby simplifying substrate preparation

Preparation of imaging samples

Substrate Preparation—Silicone (or polysiloxane) gels have previously been spin-coated in thin layers (5–10 μm) for use in TIRF.[16,17] Polymer to crosslinker ratio can be varied to obtain silicone gels of different stiffnesses.[16] The ability to deposit thin layers of these gels facilitates their adoption for use in sensitive imaging techniques. We adapt these mechanically tunable gels for mechanobiological studies using scanning angle interference microscopy. In order to coat silicon wafers with a silicone gel, we spin coated unpolymerized gel solution at 8000 rpm for 90 seconds. *N*-type (100)-orientation silicon wafers with 300nm or 1.9 μm silicon oxide (Addison Engineering) were cut into 1cmx1cm squares and cleaned in acetone, potassium chloride, and water in sequence, while sonicating, for 20 minutes each. Silicon wafer and silicon oxide deposition methods were unchanged from Paszek and colleagues' original description.[13] Mixed and degassed gel solution (Corning 52–276 Parts A and B at ratios corresponding with desired stiffness) was deposited on wafer squares using a small pipet tip or dropper before commencing the spin coating program (VTC-100, MTI Corporation). The resulting substrates were then baked at 60°C for 3 hours. To conjugate ECM proteins to the substrate surface, gels were incubated with 95% ethanol, 0.5% (3-aminopropyl)trimethoxysilane (Sigma-Aldrich) solution for 5 minutes, then 100μg/mL 1-Ethyl-3-(3-dimethylaminopropyl)carbodiimide (EDC, TCI America) + 10μg/mL human plasma fibronectin (Millipore) for 30 minutes while shaking at room temperature. At this point, samples could be stored for 1 week at 4°C or immediately used for cell seeding (Figure 1a and 1b).

Calibration Samples—To conjugate fluorescent microspheres onto the gel surface for use in calibration, gels were plasma treated (PDC-32G Plasma Cleaner, Harrick Plasma for 30 seconds after polymerization and incubated with 20μL of a 1 in 10^6 dilution of 0.1μm red fluorescent carboxylate-modified microsphere solution (Molecular Probes, Invitrogen) in the dark until dry.

Cell Samples—MCF10A human mammary epithelial cells were a generous gift from T. Tlsty (UCSF) and cultured as previously described.[13] To generate cell lines stably expressing paxillin-mCherry, paxillin-eGFP, or vinculin-eGFP, HEK-293T cells (W. Pear lab, University of Pennsylvania) were transfected with lentiviral vectors. Recombinant lentivirus was then collected and used to transduce MCF10A cells. Resulting cells were selected in media containing 200ng/mL G418 for 48 hours. Infection efficiency was verified via epifluorescence and brightfield microscopy 24 hours after doxycycline treatment. Only cell samples with >75% positive fluorescently expressing cells were used in experiments.

Cells were seeded on fibronectin-conjugated substrates on the day prior to fixation or live imaging and allowed to adapt to the gel substrate for a minimum of 18 hours. Cells used for focal adhesion or cytoskeletal component imaging were fixed in 4% paraformaldehyde in 1X Cytoskeletal Buffer (10mM MES pH6.1, 140mM KCl, 3mM MgC1_2, 2mM EGTA) supplemented with cold 11% sucrose on the day of fixation. Non-cytoskeletal component

imaging samples were fixed in 4% paraformaldehyde in PBS. In both cases, cells were fixed for 15 minutes at room temperature, washed 3 times in cold PBS, and permeabilized in 0.1% Triton-X 100 in PBS for 10 minutes. Cells were then washed three times for 15 minutes each and blocked in 1% BSA in PBS-Tween (0.3%) for one hour. Primary antibody was incubated in blocking solution overnight at 4°C. Secondary antibody was incubated in blocking solution for 1 hour, preceded and followed by three 15-minute PBS washes. Live cell imaging was achieved in an environmental chamber, at 37°C and 5% CO_2. Culture media was exchanged for imaging media (with no phenol red), to reduce background signal.

Rheology and Image Acquisition and Analysis

Shear Rheology—Shear rheology was performed on an Anton Paar Rheoplus 32 with an 8mm probe (PP08/S-SN22031). A curing test was performed at 60°C, where a 5% strain test was performed every 60 seconds until storage and loss modulus values changed by less than 1% for three consecutive time points (Supplemental Information, Figure 1). A frequency sweep between 0.5–10Hz under controlled shear deformation was then performed on the cured samples to obtain steady state storage and loss moduli. Complex modulus was then calculated using the following formula: $G^* = \sqrt{G'^2 + G''^2}$.

TIRF and SAIM—Our imaging setup consisted of a Nikon inverted TIRF microscope system (Ti-E Perfect Focus System), with 488-nm and 561-nm lasers and an electron-multiplying charged-coupled device camera (EMCCD, QuantEM 512, Photometrics). Linear light polarization was achieved as previously described.[13] To accurately correlate motor position of the TIRF illuminator with effective incidence angle of excitation, manual calibration was performed prior to each imaging session. The TIRF motor was moved to twenty-five evenly spaced out angles between −50° and +50°, and the corresponding motor position was recorded. As these angles were measured in ambient air, their corresponding angles in aqueous solutions was calculated using Snell's Law. The relationship between motor position and incident angle was fitted using a power law and the resulting equation used to calculate appropriate motor positions for acquisition angles, which ranged from −45° to +45° at 0.5° intervals. These motor units were entered into a journal in the microscope controller software (Metamorph).

Atomic Force Microscopy and Scanning Electron Microscopy—Images were acquired using a MFP3D-BIO inverted optical AFM (Asylum Research, Santa Barbara, CA) mounted on a Nikon TE200-U inverted fluorescence microscope (Melville, NY) in non-contact imaging mode. Silicon nitride cantilevers (k=0.09N/m, Olympus TR400PB) were calibrated for each session using the thermal oscillation method. Images shown are height maps of $30\mu m \times 30\mu m$ areas. All images were acquired on fresh non-fixed cells in cell culture media. For SEM, silicone gels were fixed in 1.5% glutaraldehyde/1% paraformaldehyde and impregnated with a conductive layer of osmium-thio-carbohydrazide-osmium (OTOTO). The gels were then dehydrated in a graded series of ethanol, followed by critical point drying procedure with an AutoSamdri 815 critical point dryer (Tousimis, Rockville, MD). Subsequently, the gels were imaged on JEOL JCM-6000 Neoscope Scanning Electron Microscope (JEOL USA Inc., Peabody, MA).

Image Analysis—TIFF stacks with one image corresponding to each incidence angle were processed in FIJI (NIH).[18] Stacks were z-projected with standard deviation to create a composite image, which was then binarized to generate a mask (Figure 1e). Individual TIFFs were saved for each image in the stack and input into the analysis software, along with the mask and a parameter file (Figure 1e). Raw fluorescence intensity profiles were generated in FIJI for 5 pixel x 5 pixel regions of interest and points of inflection were counted and compared with theoretically generated fluorescence intensity curves (Figure 3a and 3b). A best guess for silicone gel thickness (d_{gel}) was determined based on this comparison and input into the analysis software (Figure 1d). Both uncompiled analysis code and an example parameter file are provided as supplementary material. Analysis software was written in C++ and compiled in a Linux operating system. It makes use of the Intel Math Kernel Library for curve fitting. Visualization software was written in Python using libraries distributed by Enthought, Inc. Statistical analysis was performed in Microsoft Office Excel 2013.

Results

To evaluate the success and utility of our novel imaging platform, we identified four major design requirements:

1. the silicone gel should be mechanically tunable within a physiologically relevant range,

2. the substrate should be compatible with cell culture,

3. the silicon wafer and gel substrate should be compatible with the optical requirements of TIRF and SAIM, and

4. the new imaging system can be used to make observations about biological systems.

We address each of these design requirements in turn, in the following sections.

Substrate Rigidity and Cell Responses to Silicone Substrate

Substrate Characterization—To characterize the range of elastic moduli attainable using these silicone gels, we mixed Parts A and B of the silicone gel at varying ratios and performed shear rheology on the resulting bulk gels (Figure 2a). It is possible to generate gels from 250Pa to 100kPa, a broad range that spans the physiological range (which ranges from <1kPa in the brain to 25k–100kPa for in muscle and bone.[1,19] To further ensure the gel's compatibility with imaging requirements, we performed atomic force microscopy (AFM) and scanning electron microscopy (SEM). AFM allowed us to characterize the gel surface. Both TIRF and SAIM require relatively flat surfaces that do not induce distortions in light path. AFM imaging revealed that the gel surface had <10nm variation in height (Figure 2b). SEM suggested similar levels of roughness on the gel surface further permitted us to measure gel thickness (approximately 8μm, Figure 2c).

Biological Characterization—To investigate how cells respond on different stiffness substrates, we seeded MCF10A mammary epithelial cells (MECs) and observed cell

spreading and cell-matrix adhesion morphology. As previously reported, cell spreading was positively correlated with substrate stiffness (Figure 2d). Similarly, cells on stiff substrates (100kPa) formed large, elongated adhesions, while cells on soft substrates (250Pa) formed smaller adhesions in the middle of the cell (paxillin and actin staining, Figure 2e). These findings confirm that cells behave similarly on silicone gels as on the polyacrylamide hydrogels typically used to vary the mechanical properties of cell substrates. Further, we observed no cytotoxicity as a result of culture on silicone gels.

High-Refractive Index Silicone Gels for TIRF

To validate the refractive index of the gels and their compatibility with SAIM's optical requirements, we tested whether it is possible to perform TIRF microscopy on our silicone gel system. Specifically, we compared epifluorescent illumination with TIRF illumination of MCF10A cells expressing paxillin-mCherry and noted that, consistent with the concept of TIRF, at high incidence angles of excitation, we obtain a relative decrease in background signal and an enhancement of membrane-adjacent signal. In particular, we could much better distinguish paxillin-containing focal adhesions (Figure 2f).

Technical Validation of SAIM on Silicone Gels

Once we established that silicone gels are amenable to TIRF microscopy, we tested their compatibility with scanning angle interference microscopy. In order to do this, we needed to make theoretical adjustments to the image analysis software used to calculate fluorophore heights from acquired images. As described above, each image acquisition consists of a stack of images, each obtained at a different angle of incidence. Based on the optical theory behind SAIM, the fluorescence intensity of molecules should vary with the incident angle, in a manner that corresponds with the fluorophore's position above the reflective silicon surface.

Optical Theory—An in-depth derivation of the generalized case of this phenomenon is described by Lambacher and Fromherz in their 1996 *Applied Physics A* article.[14] Here, we describe the specific case when incident light is polarized perpendicular to the plane of incidence, as in our application of SAIM. The fluorescence intensity of a fluorophore situated at position H above a silicon surface is governed by the strength of the electric field at H. To determine the strength of this electric field, we employ the transfer matrix method, an approach to account for electromagnetic waves of a given frequency propagating through a stack of layers of different materials.[20] It is based on the idea that, according to Maxwell's equations, there exist continuity conditions for an electric field as it crosses boundaries from one medium to another. Essentially, this means that if the field is known at the beginning of a layer, it is possible to calculate the field at the end of the layer through a matrix operation. Each layer has its corresponding transfer matrix, which can be multiplied together to produce the system matrix.

Each layer's transfer matrix is calculated using Fresnel coefficients. The standard form for a transfer matrix is as follows:

$$\begin{pmatrix} \cos(kL) & \frac{1}{k}\sin(kL) \\ -ksin(kL) & \cos(kL) \end{pmatrix}$$

where k is the wave number in the material, and L is distance traversed through the material.

Hence, for the silicon + silicon oxide case, the characteristic transfer matrix is

$$M_{TE} = \begin{pmatrix} m_{11}^{TE} & m_{12}^{TE} \\ m_{21}^{TE} & m_{22}^{TE} \end{pmatrix}$$
$$= \begin{pmatrix} \cos(k_{ox}d_{ox}cos\theta_{ox}) & -\frac{i}{p_{ox}}\sin(k_{ox}d_{ox}cos\theta_{ox}) \\ -ip_{ox}\sin(k_{ox}d_{ox}cos\theta_{ox}) & \cos(k_{ox}d_{ox}cos\theta_{ox}) \end{pmatrix}$$

where $p_{ox} = n_{ox}\cos\theta_{ox}$, $k_{ox} = \frac{2\pi n_{ox}}{\lambda}$, for light wave with wavelength λ. $d_{ox}cos\theta_{ox}$ stands in for L, by taking into account the true thickness of the layer, d_{ox}, as well as the angle at which the light travels through the layer, θ_{ox}.

When we add in the silicone gel layer, we must include its corresponding transfer matrix:

$$= \begin{pmatrix} \cos(k_{gel}d_{gel}cos\theta_{gel}) & -\frac{i}{p_{gel}}\sin(k_{gel}d_{gel}cos\theta_{gel}) \\ -ip_{gel}\sin(k_{gel}d_{gel}cos\theta_{gel}) & \cos(k_{gel}d_{gel}cos\theta_{gel}) \end{pmatrix}$$

with $p_{gel} = n_{gel}\cos(\theta_{gel})$ and $k_{gel} = \frac{2\pi n_{gel}}{\lambda}$.

If we substitute $l_{gel} = k_{gel}d_{gel}\cos(\theta_{gel})$ and $l_{ox} = k_{ox}d_{ox}\cos\theta_{ox}$ and multiply the silicon oxide transfer matrix by the silicone gel matrix, we obtain the system matrix with the following components:

$$m_{11}^{TE} = \cos(l_{gel})\cos(l_{ox}) - \frac{p_{ox}}{p_{gel}}\sin(l_{gel})\sin(l_{ox})$$
$$m_{12}^{TE} = -\frac{i}{p_{ox}}\cos(l_{gel})\sin(l_{ox}) - \frac{i}{p_{gel}}\sin(l_{gel})\cos(l_{ox})$$
$$m_{21}^{TE} = -ip_{gel}\sin(l_{gel})\cos(l_{ox}) - ip_{ox}\cos(l_{gel})\sin(l_{ox})$$
$$m_{22}^{TE} = -\frac{p_{gel}}{p_{ox}}\sin(l_{gel})\sin(l_1) + \cos(l_{gel})\cos(l_{ox})$$

This can then be used to construct the transverse electric component (perpendicular to the plane of incidence) of the Fresnel coefficient of reflection between the imaging substrate and the sample:

$$r^{TE} = \frac{(m_{11}^{TE} + m_{12}^{TE}p_0)p_2 + (m_{21}^{TE} - m_{22}^{TE}p_0)}{(m_{11}^{TE} + m_{12}^{TE}p_0)p_2 + (m_{21}^{TE} + m_{22}^{TE}p_0)}$$

where $p_0 = n_{si}\cos\theta_{si}$, $p_2 = n_s\cos\theta_s$, corresponding to the silicon and sample layers, respectively.

This, in turn, allows us to know what happens to the electric field strength as it passes through each material in our experimental system. Generally, it can be calculated as follows:

$$F \approx 1 + r^{TE}e^{i\phi(H)}$$

where ϕ is the phase difference between the direct and reflected light at position H:

$$\phi(H) = \frac{4\pi}{\lambda}(n_s H \cos\theta_s)$$

for a light wave with wavelength λ at angle θ_s through a sample with refractive index n_s.

The analysis software uses constrained nonlinear least-squares optimization to fit experimental fluorescence intensity profiles to theoretically predicted profiles on a pixel by pixel basis. Fluorescence emission is proportional to the excitation radiation intensity, which is proportional to the squared projection of the local electric field onto the normal plane:

$$I = A\left|1 + r^{TE}e^{i\phi(H)}\right|^2 + B$$

where A adjusts for variation in intensity due to contributions from mean excitation laser intensity, fluorophore properties, and the efficiency of emitted photon detection and B accounts for background signal in the sample. The fitting algorithm fits for the parameters *A, B,* and *H.*

Fluorescent Microsphere Validation—To test whether this new optical model can correctly calculate the position of a fluorophore above the silicon, silicon oxide, and silicone gel substrate, we conjugated fluorescent microspheres of known size onto the gel surface. Multiple quality control processes were employed both before and after quantitative image analysis. To account for variations in spin coated gel thickness, experimental fluorescence intensity curves were compared with a range of computationally generated curves to find the approximate range of gel thickness. Figure 3a illustrates how experimentally obtained pixel intensity can be plotted against excitation angle. The resulting curve can be used to evaluate instrument calibration. If TIRF angle calibration has been performed correctly, the curve should be mirrored around zero degrees and exhibit a periodic pattern as incidence angle changes. This experimental profile can be compared to the regular patterns of oscillation predicted by the optical model (Figure 3b). This process is performed with each set of experiments. A second quality control step is specifically implemented for microspheres. Due to the possibility of microsphere aggregates, masks are generated in FIJI using z-projection with standard deviation. This allows isolation and exclusion of brighter than average bead clusters. Only values below 75% of maximum brightness are kept for mask generation. Finally, after image analysis, all pixels with an A-value less than 1.5 times the average A value for the experimental set are excluded. This necessarily leads to low yield

but decreases neighbouring pixel variability and whole cell variability. Figure 3c compares summarized height distributions from 6 microsphere samples imaged on either a 1900nm thick silicon oxide surface (left) or a spin-coated silicone gel surface (right). Microspheres with radius 50nm were used. SAIM calculations represent an average of all fluorescent signal in a given pixel. In the case of fluorescent microspheres, we detect fluorescent signal at all heights between 0 and 100nm and would expect the calculated height at a pixel to be 50nm—the center of the fluorescent signal detected. While there is less variation in the silicon oxide case, imaging on silicone gel substrates still produced reproducibly accurate height calculations, with an average near 50nm. This validates our ability to perform SAIM on silicone gels and to accurately measure the height of objects of known size above the imaging surface.

Biological Validation of SAIM on Silicone Gels—To evaluate and demonstrate compatibility of this method to use in biological study, we used this silicone-gel SAIM to image focal adhesion and cytoskeletal protein positioning within MECs. Figure 3d–f provides examples of representative images in the analysis process: the raw z-projected fluorescence image (3d), a masked image with areas of interest (adhesion) shown in white (3e), and a color map of adhesion heights produced after image analysis and fitting (3f). One indicator of high quality SAIM imaging and proper fitting is low variation in height in a local area, such as within an adhesion. The analysis software calculates height for each pixel independently. Hence, there is no memory or expectation of local agreement in height written into the program. As such, if we find that our results suggest an adhesion, made up of many pixels, is at approximately the same height above the substrate, this suggest that the method has been implemented correctly. Essentially, we use our biological intuition to evaluate technical execution of the method. For this first test, we imaged GFP-tagged vinculin and found it to be positioned approximately 60–90 nm above the cell substrate. This compares favourably with previously published studies, wherein vinculin z-position was imaged with PALM[21] and SAIM[13]. These studies reported finding vinculin between 45–60nm using PALM and 80–100nm using SAIM.

To demonstrate the potential for this novel platform to provide biological insight, we compared positions of two focal adhesion proteins in cells cultured on stiff and soft substrates. To facilitate direct comparison and to illustrate how this method could be used to study the relative positions of proteins within focal adhesions, we imaged both vinculin and paxillin in the same cells. We find that vinculin position does not change significantly. Its range on soft substrates is tightly distributed around 100nm, with 95% of observations falling between 60nm and135nm (Figure 4a, individual example, and 4c, aggregated data). Vinculin height in cells on stiff substrates centered around 86nm and 95% of observations fell between 68nm and 112nm (Figure 4b, individual example, and 4d, aggregated data). In contrast, while paxillin position averages 66nm on stiff substrates, (Figure 4b and 4d), its heights exhibit a clear, bimodal distribution on soft substrates(Figure 4a and 4c). This shift could be the result of changing binding partners for paxillin or a larger reorganization of the adhesion. Elucidating the precise mechanisms underlying this shift will certainly require further manipulation and study, but this intriguing example points to the types of phenomena this method could help to unveil and investigate.

To further explore ways in which this method may be used for biological investigation, we performed time-lapse SAIM imaging on MCF10A cells expressing paxillin-GFP (Figure 5a). With 100ms exposure time, a full set of 182 frames required less than 50s for acquisition. This short acquisition time permits capturing dynamic cell processes, such as adhesion disassociation and maturation, which happen on a length scale of minutes. For instance, focal adhesion disassembly occurs over the course of 10–20 minutes.[22] In this example, we can see one population of paxillin disappear as a part of the membrane retracts and new adhesions form (Figure 5b and 5c, arrows).

Benchmarking—Implementation of SAIM on mechanically tunable gels affords the ability to achieve 30–40nm precision in determining protein localization in z. This compares favourably to conventional confocal laser scanning microscopy, which has z-resolution in the range of 500–700nm.[23] Currently commercially available microscopy setups include stimulated emission depletion (STED), structured illumination microscopy (SIM), and PALM/STORM, as previously described.[23] These methods can achieve lateral resolution in the 30–150nm range, but are far more limited in z, from 140nm for PALM/STORM to 250nm in SIM, and 500–700nm in STED.[23] Of these methods, methods that allow penetrance into thick samples, like confocal or structured illumination microscopy, sacrifice vertical resolution. In contrast, methods that afford higher vertical resolution, like PALM/STORM, sacrifice compatibility with physiologically relevant samples. Uniquely, implementation of SAIM on mechanically tunable gels offers the ability to perform experiments on physiologically relevant samples while maintaining state of the art vertical resolution.

Summary

There remain many unanswered questions regarding how the mechanical properties of the extracellular matrix influence and regulate cellular processes. Use of novel nanoscale imaging techniques has already allowed researchers to elaborate many intricate signalling phenomena. This new method will facilitate application of one such tool to mechanobiological investigation. In addition to studying the nanoscale organization of focal adhesion proteins and the cytoskeleton, this method could be applied to study membrane curvature and topology under different substrate contexts, the interaction of membrane lipids and proteins, and more. The application of SAIM on mechanically tunable substrates combines physiologically relevant substrates with state of the art superresolution imaging, while affording the ability to perform live cell tracking. We present a method that can be implemented on commercially available microscopy equipment, with open-source analysis software, and with little investment in special materials. We look forward to its adoption and implementation to broaden our understanding of the effect of ECM rigidity on a wide array of cellular processes.

Supplementary Material

Refer to Web version on PubMed Central for supplementary material.

Acknowledgments

References

1. Engler AJ, Sen S, Sweeney HL, Discher DE. Cell. 2006; 126:677–689. [PubMed: 16923388]

2. Paszek MJ, Zahir N, Johnson KR, Lakins JN, Rozenberg GI, Gefen A, Reinhart-King CA, Margulies SS, Dembo M, Boettiger D, Hammer DA, Weaver VM. Cancer Cell. 2005; 8:241–254. [PubMed: 16169468]

3. Butcher DT, Alliston T, Weaver VM. Nat Rev Cancer. 2009; 9:108–22. [PubMed: 19165226]

4. Klein EA, Yin L, Kothapalli D, Castagnino P, Byfield FJ, Xu T, Levental I, Hawthorne E, Janmey PA, Assoian RK. Curr Biol. 2009; 19:1511–8. [PubMed: 19765988]

5. Zhang YH, Zhao CQ, Jiang LS, Dai LY. Matrix Biol. 2011; 30:135–44. [PubMed: 21055467]

6. Welsh CF, Roovers K, Villanueva J, Liu Y, Schwartz MA, Assoian RK. Nat Cell Biol. 2001; 3:950–957. [PubMed: 11715015]

7. Price LS, Leng J, Schwartz MA, Bokoch GM. Mol Biol Cell. 1998; 9:1863–1871. [PubMed: 9658176]

8. Thakar RG, Chown MG, Patel A, Peng L, Kumar S, Desai TA. Small. 2008; 4:1416–1424. [PubMed: 18711756]

9. Burdick JA, Prestwich GD. Adv Mater. 2011; 23:H41–H56. [PubMed: 21394792]

10. Shroff H, Galbraith CG, Galbraith JA, Betzig E. Nat Methods. 2008; 5:417–23. [PubMed: 18408726]

11. Paszek MJ, DuFort CC, Rossier O, Bainer R, Mouw JK, Godula K, Hudak JE, Lakins JN, Wijekoon AC, Cassereau L, Rubashkin MG, Magbanua MJ, Thorn KS, Davidson MW, Rugo HS, Park JW, Hammer DA, Giannone G, Bertozzi CR, Weaver VM. Nature. 2014; 511:319–25. [PubMed: 25030168]

12. Doksani Y, Wu JY, de Lange T, Zhuang X. Cell. 2013; 155:345–56. [PubMed: 24120135]

13. Paszek MJ, DuFort CC, Rubashkin MG, Davidson MW, Thorn KS, Liphardt JT, Weaver VM. Nat Methods. 2012; 9:825–7. [PubMed: 22751201]

14. Lambacher A, Fromherz P. Appl Phys A. 1996; 63:207–216.

15. Ajo-Franklin CM, Ganesan PV, Boxer SG. Biophys J. 2005; 89:2759–69. [PubMed: 16085775]

16. Gutierrez E, Tkachenko E, Besser A, Sundd P, Ley K, Danuser G, Ginsberg MH, Groisman A. PLoS One. 2011; 6:e23807. [PubMed: 21961031]

17. Koschwanez JH, Carlson RH, Meldrum DR. PLoS One. 2009; 4:e4572. [PubMed: 19238212]

18. Schindelin J, Arganda-Carreras I, Frise E, Kaynig V, Longair M, Pietzsch T, Preibisch S, Rueden C, Saalfeld S, Schmid B, Tinevez JY, White DJ, Hartenstein V, Eliceiri K, Tomancak P, Cardona A. Nat Methods. 2012; 9:676–82. [PubMed: 22743772]

19. Levental I, Georges PC, Janmey PA. Soft Matter. 2007; 3:299–306.

20. Katsidis CC, Siapkas DI. Appl Opt. 2002; 41:3978–87. [PubMed: 12099609]

21. Kanchanawong P, Shtengel G, Pasapera AM, Ramko EB, Davidson MW, Hess HF, Waterman CM. Nature. 2010; 468:580–4. [PubMed: 21107430]

22. Webb DJ, Donais K, Whitmore LA, Thomas SM, Turner CE, Parsons JT, Horwitz AF. Nat Cell Biol. 2004; 6:154–61. [PubMed: 14743221]

23. Schermelleh L, Heintzmann R, Leonhardt H. J Cell Biol. 2010; 190:165–75. [PubMed: 20643879]

Insight box

The mechanical properties of the extracellular matrix are recognized as an important mediator of cell signaling and function. Existing nanometer-scale imaging methods depend on the use of artificially rigid substrates that prevent researchers from drawing physiologically relevant conclusions. We present a novel imaging platform that addresses this gap in technology and demonstrate its potential for use in biological study. This mechanically tunable silicone gel system for scanning angle interference microscopy affords the ability to specify focal adhesion or cytoskeletal protein localization within the cell to nanometer precision and will facilitate elucidation of the molecular mechanisms underlying mechanotransduction. Further, this method may be used to study how changing mechanical cues affects canonical cell signaling and protein organization within the cell.
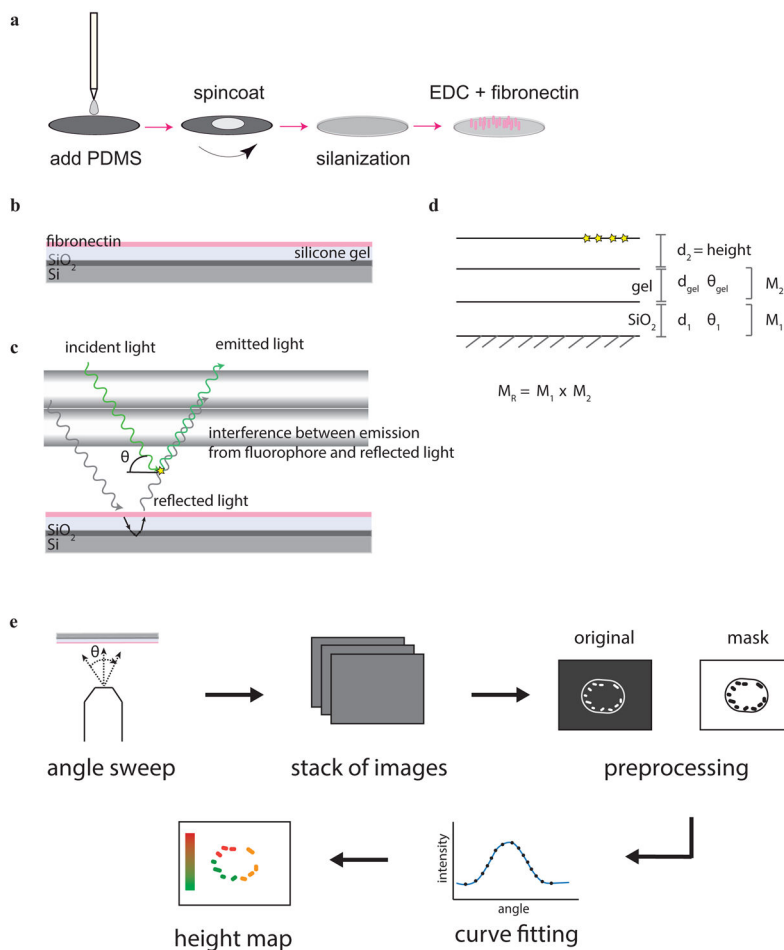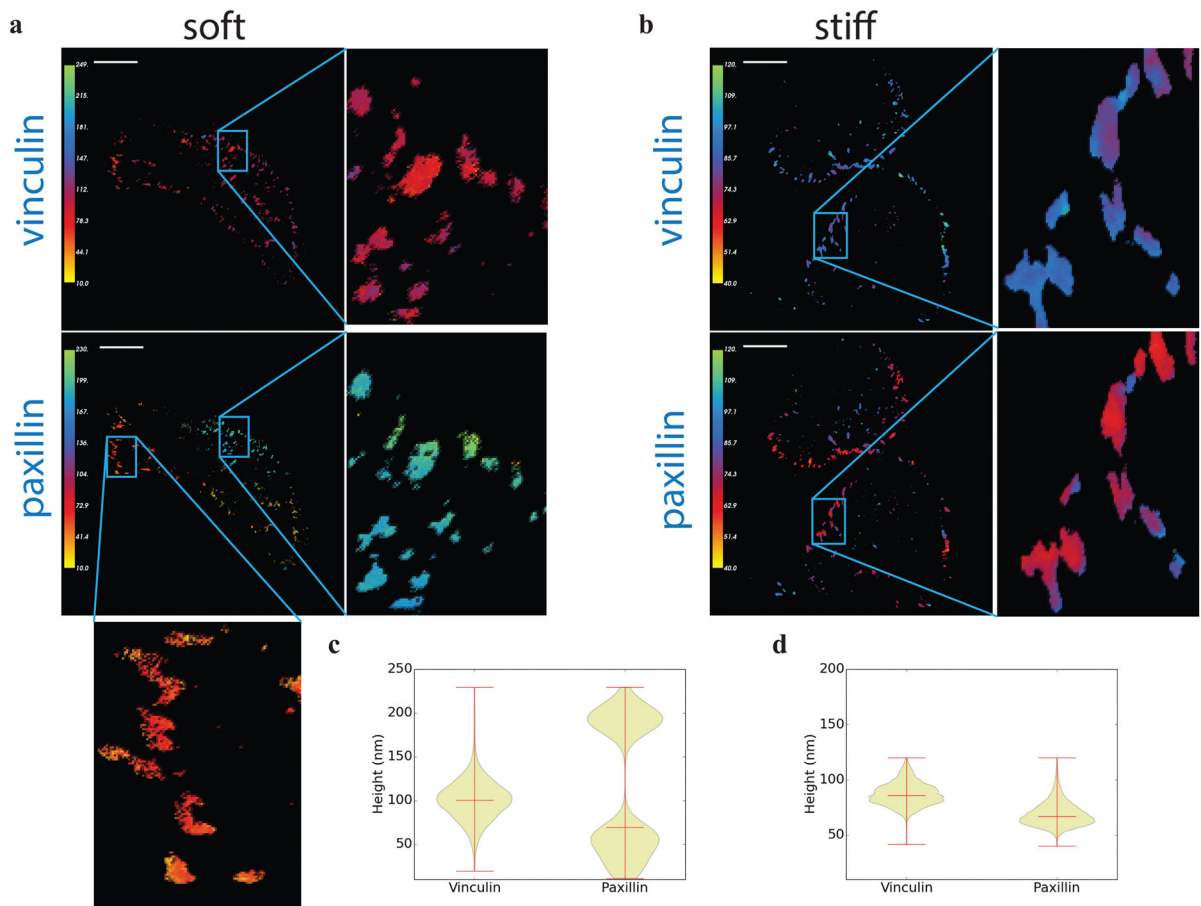
Figure 1.
experimental setup. a) spin coating and activation procedure. b) gel and silicon wafer layout. c) optical theory behind scanning angle interference microscopy (saim). reflected excitation light interferes with emission from fluorophore in a manner that is dependent on the angle (θ) of incidence of excitation light. this interference pattern can be used to calculate the height of a fluorophore situated above the substrate surface, as illustrated in d). here, we consider the silicon oxide as one layer and the gel as another layer. knowing the thickness (d_1 or d_{gel}) of the materials and angle of light passage (θ) through these materials allows us to construct transfer matrices (m_1 and m_2) and solve for d_2, the fluorophore height. adding multiple layers together means multiplying their respective transfer matrices to obtain a system transfer matrix, m_r. see text for full derivation. e) an overview of the acquisition and analysis process. a sample is imaged at multiple angles of incidence, producing a stack of images in which each image corresponds with one angle of incidence. this stack is used to generate a mask of regions and feature of interest, which is then used by the analysis software to determine which pixels to analyze. the software compares experimental intensity vs. incidence angle curves to those predicted by optical theory and finds the best fit for each pixel. the output of this analysis is a height map that reflects the best fit angle for each pixel indicated in the mask.
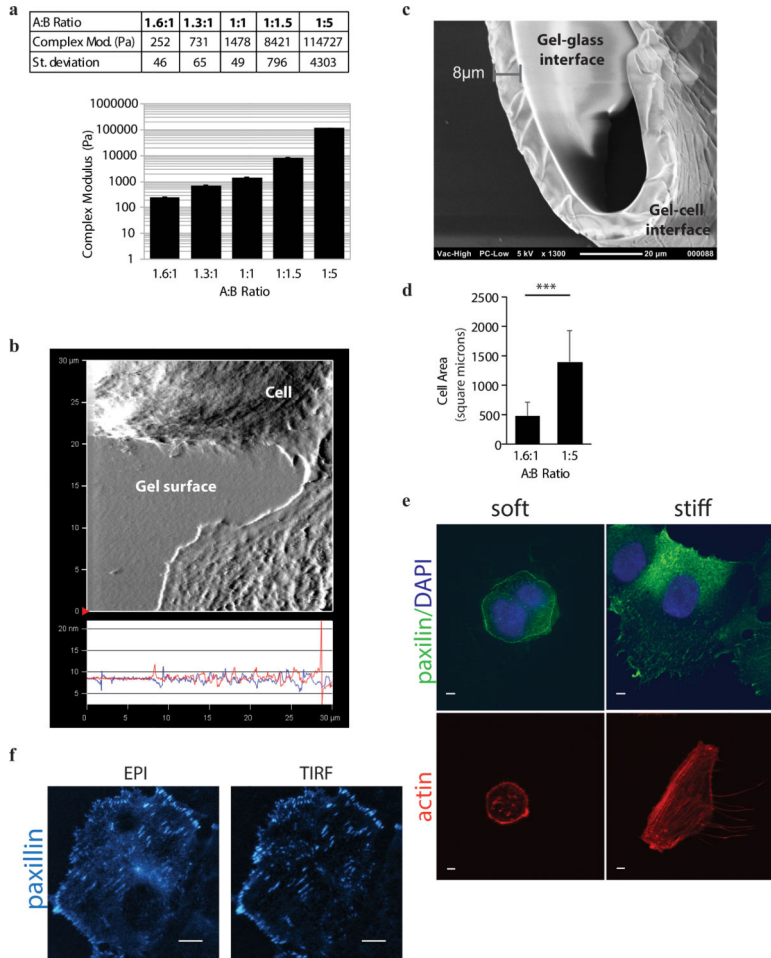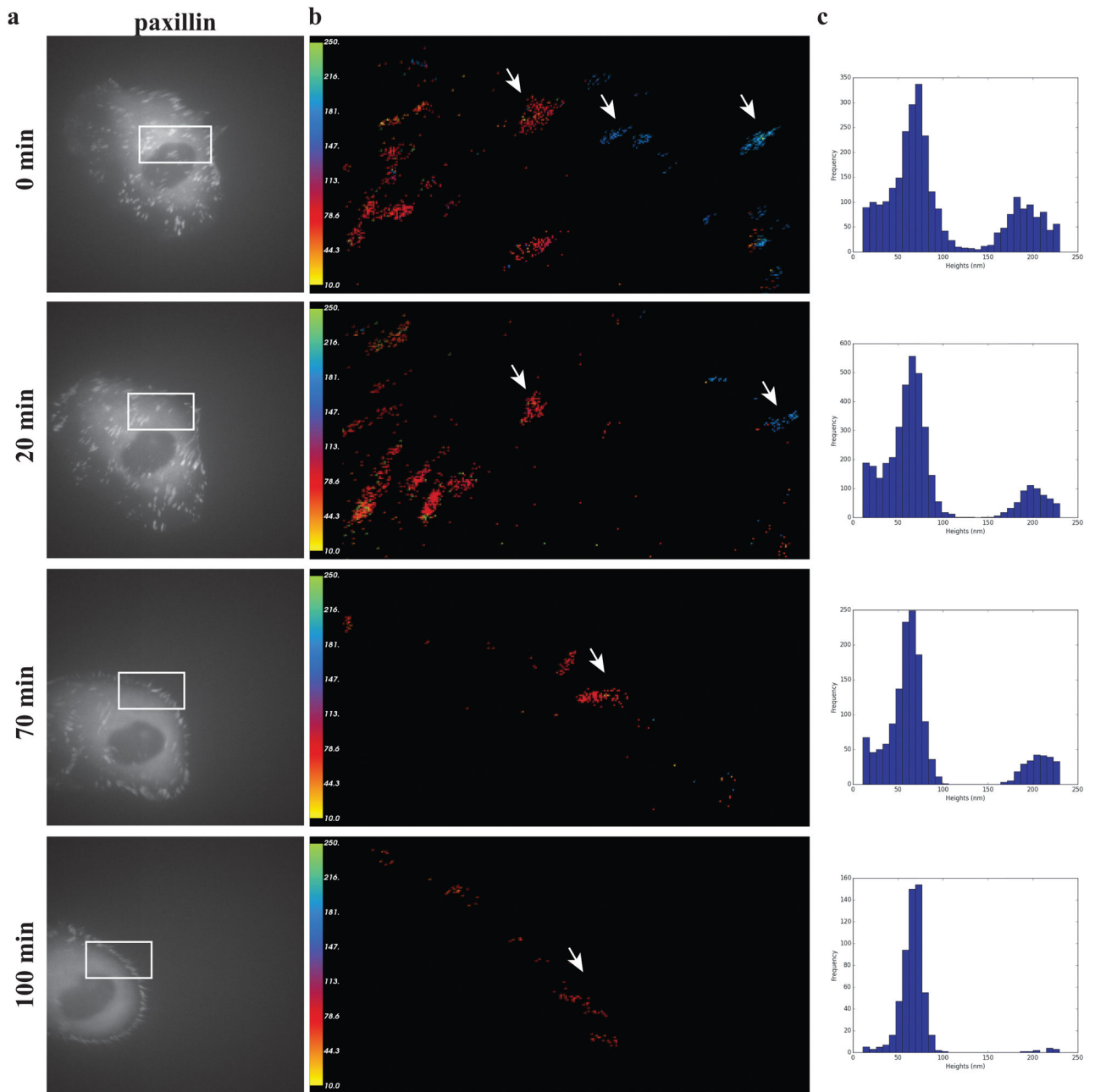
Figure 2.

silicone gel characterization. a) shear rheology of different gel base (a) to crosslinker (b) ratios and corresponding complex modulus. b) atomic force microscopy image of epithelial cell seeded on matrix-protein functionalized silicone gel. c) scanning electron microscopy of detached gel that allows characterization of gel surface roughness and thickness. d) biological characterization of cellular response on gels with a:b ratios as indicated. cells are more spread, as expected, on stiffer gels. asterisks indicates p< 0.005. e) confocal fluorescence microscopy of paxillin-gfp expressing mcf10a cells immunostained with dapi and alexafluor594-phalloidin on soft (252pa) and stiff (114kpa) gels. scale bar = 4.5μm. f) paxillin-mcherry mcf10a cells seeded on stiff gels imaged under epifluorescence (left) and tirf (right). scale bar = 4.5μm.
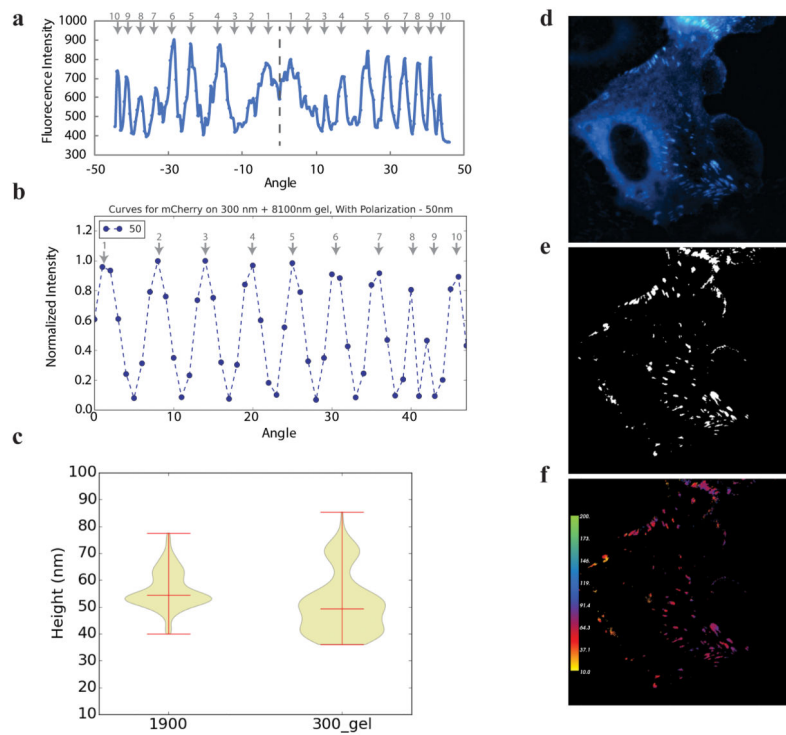
Figure 3.
technical and biological validation of saim on silicone gels. a) an example of an experimentally obtained fluorescence intensity profile. dotted line indicates incidence angle = 0°. note that the profile is mirrored around this angle. arrows indicate each inflection point and allows comparison with b) computationally generated curves. c) comparison of fluorescence microsphere height on substrates without silicone gel (left) and with gel (right). d–f) example of image processing process, with raw image (d), mask (e), and height map (f) of a vinculin-egfp expressing mcf10a cell.

Figure 4.
further biological validation of saim on silicone gels. a) height maps of paxillin and vinculin in the same mcf10a cell on soft gel substrate, with insets. b) height maps of paxillin and vinculin in the same mcf10a cell on stiff, silicon oxide substrate, with insets. c) violin plot of adhesion protein heights for cells on soft substrates. d) violin plot of adhesion protein heights for cells on stiff, silicon oxide substrates. scale bar = 3μm.

Figure 5.
time-lapse imaging with saim. a) z-projected images from time-lapse saim imaging of a migrating paxillin-egfp expressing mcf10a cell on a 1.5kpa silicone gel substrate at 0, 20, 70, and 100minutes, with b) height maps for the areas boxed in white and c) histograms of height distributions in these cells. arrows point out representative adhesions as the cell migrates. note how the blue (approximately 190nm) population disappears as the cell migrates.